Materials Science Forum
ISSN: 1662-9752, Vol. 1092, pp 187-192
doi:10.4028/p-0y444y

Submitted: 2022-09-04
Revised: 2022-11-04
Accepted: 2022-11-25
Online: 2023-06-06

Energy-Dependent Impact of Proton Irradiation on 4H-SiC Schottky Diodes

P. Kumar[1,a,*], M. Belanche[1,b,**], N. Für[1,c,**], L. Guzenko[1,d], J. Woerle[1,e], M. E. Bathen[1,f] and U. Grossner[1,g]

[1]Advanced Power Semiconductor Laboratory, ETH Zürich, Physikstrasse 3, 8092 Zürich, Switzerland

[a]kumar@aps.ee.ethz.ch, [b]mbelanche@aps.ee.ethz.ch, [c]nfuer@student.ethz.ch, [d]lguzenko@student.ethz.ch, [e]woerle@aps.ee.ethz.ch, [f]bathen@aps.ee.ethz.ch, [g]ulrike.grossner@ethz.ch

[**]These authors contributed equally to the work.

Keywords: Proton Irradiation, Energy Dependence, 4H-SiC, Schottky Barrier Diodes, Point Defects, DLTS, MCTS.

Abstract. In this work, the impact of 200 MeV proton irradiation at a fluence of 6×10^{12} cm^{-2} on the forward characteristics and the breakdown behaviour of nickel (Ni) and titanium (Ti) Schottky barrier diodes is explored. An improvement in the ideality factor, reduction in the threshold voltage, and an increase in the breakdown voltage is observed post irradiation. Point defects induced by the irradiation are likely responsible for the observed effects. Deep Level Transient Spectroscopy (DLTS) and Minority Carrier Transient Spectroscopy (MCTS) measurements were performed on the irradiated Schottky diodes to analyse the defects created during the irradiation and gauge their potential role in changing the diode behaviour. The defects induced by the high-energy protons were compared to those formed by low-energy proton irradiation at 1.8 MeV to a fluence of 1×10^{12} cm^{-2}. Finally, consecutive DLTS measurements were performed after a series of reverse bias anneals at low temperatures from 350-700 K to explore the annealing behaviour of the defects induced by the proton irradiations.

Introduction

Silicon carbide (SiC) is one of the most important semiconducting materials in the field of power electronics. In addition to its large band gap, high thermal conductivity and high saturation velocity [1], 4H-SiC has a high tolerance to radiation and finds applications in harsh environments [2]. After proton irradiation, changes in the electrical behaviour of 4H-SiC are observed [3,4] along with the creation of point defects [5], some of which are viable candidates for future quantum technology applications [6]. On the other hand, changes in electrical parameters, due to point defects, may also lead to carrier trapping, increased leakage current, and reduction in minority carrier lifetimes. It has been further observed that the existence of deep levels, which are associated with proton irradiation, affect the majority carriers in Schottky barrier diodes (SBD) [7,8].

The aim of this paper is to explore the impact of irradiation on the electrical characteristics of the SBDs and how this links to defect formation in the diode's drift layer. In this context, an understanding of the nature of the defects created during the irradiation and their annealing behaviour at low temperatures are needed. In this work, 4H-SiC SBDs were irradiated with 200 MeV protons while 4H-SiC epitaxial layers were irradiated with 1.8 MeV protons to compare defect formation by fast and slow protons. The SBDs were characterised electrically before and after the proton irradiation to observe the impact on the forward and reverse characteristics of the diodes. Further, detailed DLTS measurements were performed to extract information about the damage caused by proton irradiation.

Experimental Details

N-doped and n-type 4H-SiC samples with 10 μm epitaxial layers and a background doping concentration of 3×10^{15} cm^{-3} are used for the fabrication of the SBDs, which were proton irradiated at 200 MeV. A thin layer of thermal oxide and a subsequent layer of deposited oxide (using PECVD)

are used as field oxides. The first set consisting of three samples have 150 nm thick circular Ni contacts while the second set has 150 nm thick circular Ti contacts. The contacts have radii ranging from 80-300 μm. To observe the dependency of the breakdown voltage on the field oxide thickness, samples with 0 nm, 50 nm and 100 nm of deposited oxide are prepared for each set. Ni is deposited on the C-face for all the samples to obtain an ohmic contact. The details of the sample processing is shown in Table 1. For the sample irradiated with low energy (1.8 MeV) protons, a $10\,\mu$m thick epi-layer having 1×10^{15} cm^{-3} background doping as determined by C-V measurements was employed. The free carrier density was reduced to 6.44×10^{14} cm^{-3} at 300 K after 1.8 MeV proton irradiation. 150 nm thick Ni Schottky contacts of 600 μm diameter are deposited on top of 20 nm thick (semi-transparent) and 1500 μm diameter contact. Silver paste is used as a back contact. The semi-transparent contact allows to perform minority carrier transient spectroscopy using a LED.

DLTS measurements were performed at a reverse bias of -5 V and pulsed to 0 V. A pulse width (t_p) of 100 ms is used for a constant period width (T_W) of 500 ms. During MCTS measurements, a 365 nm LED is used at an output power of 200 mW. The DLTS and MCTS signals shown in the present paper refer to the coefficient of the sine term (b_1) in the Fourier series of the deep level transient Fourier spectroscopy (DLTFS) [9].

Table 1: Description of the processing steps for the 4H-SiC Schottky diodes irradiated with 200 MeV protons.

Sample name	Metal deposited	Thermal oxide thickness	PECVD oxide thickness
Ni-01, Ni-02, Ni-03	Nickel (Ni)	20 nm	0 nm, 50 nm, 100 nm
Ti-01, Ti-02, Ti-03	Titanium (Ti)	20 nm	0 nm, 50 nm, 100 nm

Electrical Characterisation

The Schottky diodes have been electrically characterized before and after irradiation (200 MeV) and comparison of the parameters in the on and the off state has been performed. Using the forward current-voltage (I-V) measurements, the barrier height (ϕ_{b0}), ideality factor (n), and threshold voltage (V_{th}) have been extracted. As shown in Fig. 1 a), after irradiation an improvement in the ideality factor is observed for both the Ni-02 and Ti-02 samples. Further, Fig. 1 b) and c) demonstrate a reduction in the V_{th} and an increase in the ϕ_{b0} after irradiation. These changes in the forward characteristics of the diode could be a result of deep level defects created in the bulk of the sample along with the changes near the metal-semiconductor interface. This shall be further explored in the subsequent sections.

Fig. 2 depicts the breakdown voltage recorded for the six SBDs before and after the 200 MeV proton irradiation. Solid red and blue lines are used to highlight the maximum recorded breakdown voltage in each sample and perform a comparison across the samples before and after irradiation. For all the six diodes, an increase in breakdown voltage is recorded after the irradiation which has also been predicted in literature using TCAD simulations [7]. As the area of the contact increases, a reduction in the breakdown voltage is observed for the irradiated samples. Further, a direct relation between the breakdown voltage and the thickness of the deposited oxide layer is found, where for the non-irradiated samples the breakdown voltage increases with the field oxide thickness. The set of samples with Ni as the Schottky contact exhibits a higher breakdown voltage when compared to the second set with Ti as the Schottky contact. This can be attributed to a lower barrier height for diodes with Ti as the Schottky metal [1].

DLTS Measurements

To understand the nature of defects created during the irradiation and their annealing behaviour at low temperatures, DLTS measurements are performed on one of the 200 MeV irradiated samples (Ni-01). Multiple rounds of measurements are performed starting from 50 K. The upper limit of the temperature is kept to 300 K in the first round and increased by 100 K in subsequent rounds of measurements until 700 K. Further, in order to explore the impact of the energy of the incident particles on the created

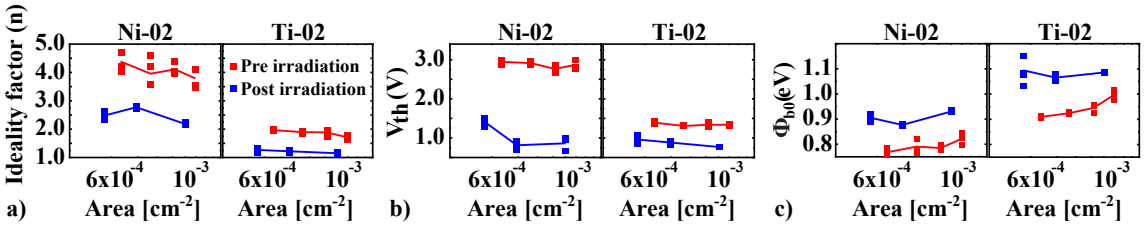

Fig. 1: Comparison of the a) ideality factor, b) threshold voltage and c) built-in potential of the Schottky diodes before and after irradiation with protons of 200 MeV.

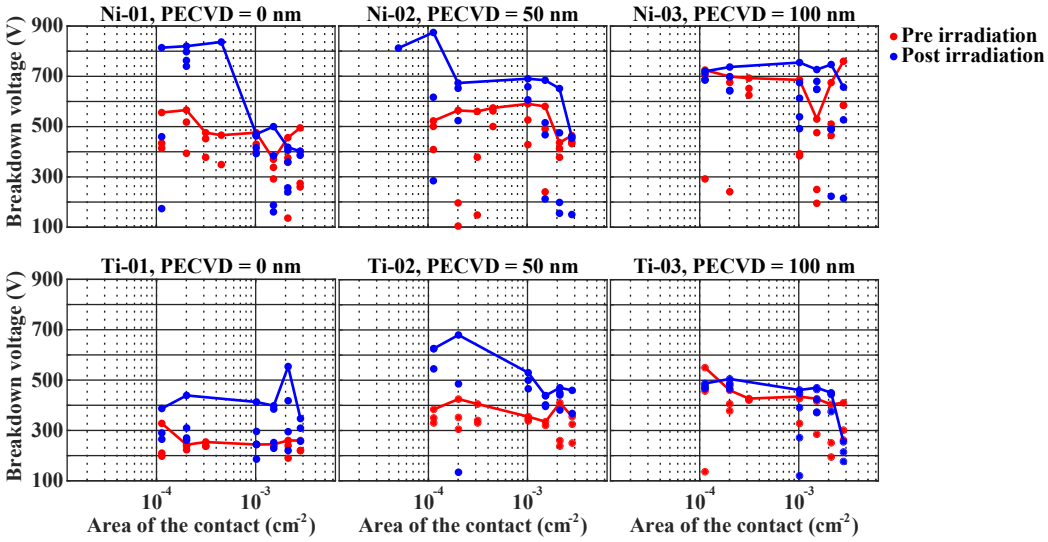

Fig. 2: Breakdown voltage measured for the Schottky diodes irradiated with 200 MeV protons to a fluence of 6×10^{12} cm^{-2}.

defects, we have also performed a similar measurement on the low-energy (1.8 MeV) proton irradiated sample. The measured spectrum for both the samples are shown in Figure 3 and the details of the extracted defects are shown in Tables 2 and 3, respectively, for the high- and low-energy irradiation. For both the samples, similar defects are created after proton the irradiation. The dominant defect centers in both sample types (200 and 1.8 MeV protons) are S1 (0.4 eV), S2 (0.7 eV), $Z_{1/2}$ (0.64-0.68 eV), $EH_{4/5}$ (1.1 eV) and $EH_{6/7}$ (1.55 eV). Similar defect levels have been reported in literature after proton irradiation [10,11]. The S1 and S2 levels have been assigned to the (2-/3-) and (-/2-) energy levels of the silicon vacancy (V_{Si}) [6], the $Z_{1/2}$ originates from the (0/2-) negative-U transition and the $EH_{6/7}$ from the (2+/+/0) transition of the carbon vacancy (V_C) [12], while EH_4 and EH_5 were recently tentatively assigned to the (+/0) charge transition level of the carbon antisite-vacancy pair ($C_{Si}V_C$) [13] Although the defect types are similar after high and low energy proton irradiation, the concentration of defects recorded in the samples is very different as illustrated by the SRIM profiles in Fig. 4 that were calculated for the proton energies used. At 1.8 MeV (Fig. 4 a)), the protons are expected to stop at $\sim$27 μm into the sample creating defects along its path. The inset shows a near-constant V_{Si} and V_C concentration profile in the first 10 μm of the sample where the DLTS measurements are performed. The concentration of the defects extracted from the DLTS measurement for the two defects is similar to the value obtained from the SRIM simulation assuming a 3 % dynamic annealing survival rate [6] (see Table 3). At 200 MeV, the protons traverse the entire region (360 μm) and do not interact much with the sample, leading to lower defect concentration in the region probed by DLTS. However, the high energy proton irradiation creates defects in the entire epitaxial layer and the 350 μm thick substrate, creating a high resistance path for the current. This could potentially be the reason for an increase in the breakdown voltage after irradiation with 200 MeV protons as shown in Fig. 2.

A change in the DLTS spectrum can be observed for each temperature scan, illustrating the impact of low temperature annealing on the defects created during proton irradiation. The impact of low

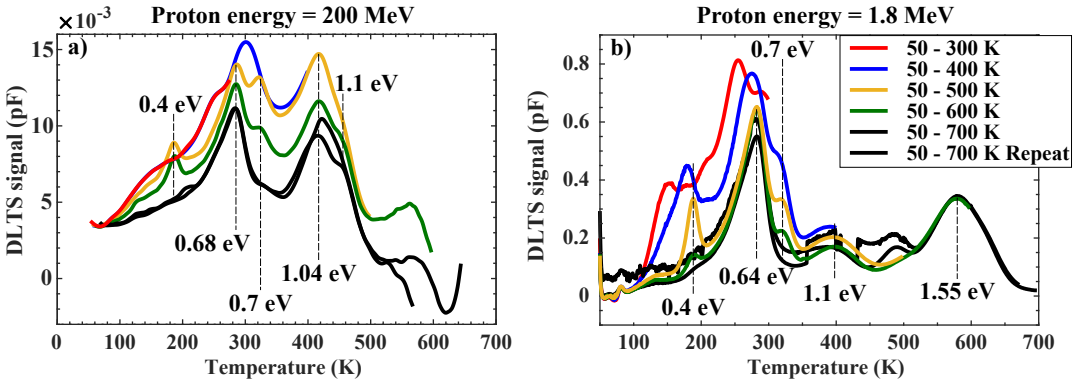

Fig. 3: DLTS spectra recorded for 4H-SiC samples irradiated with protons of a) 200 MeV energy and a fluence of 6×10^{12} cm^{-2} and b) 1.8 MeV energy and a fluence of 8×10^{11} cm^{-2}.

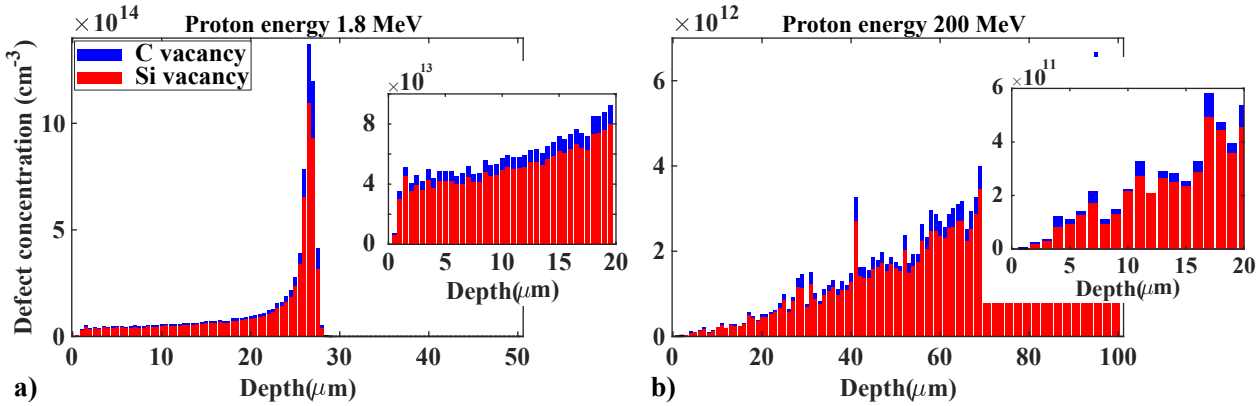

Fig. 4: SRIM simulation of generated C and Si vacancies after irradiation with protons at a) 1.8 MeV and b) 200 MeV. The insets shows the concentration of defects in the epitaxial layer of the two samples, where the defect concentration is almost an order of magnitude smaller for the 200 MeV proton irradiated sample.

temperature annealing is more pronounced for the low energy proton irradiated sample and therefore a more detailed DLTS measurement with smaller temperature steps (25 K) was performed. MCTS measurements were also performed to observe the behaviour of the minority carrier traps generated after proton irradiation. The results are shown in Fig. 5 where a)-c) show the DLTS spectrum and d)-f) the MCTS spectrum. The activation energy of each trap is indicated in the plots.

Fig. 5 a) shows the defect levels present in a non-annealed irradiated sample, the variation of these levels with temperature, and the appearance of new levels with low-temperature annealing up to 400 K. Defect levels at 0.18 eV, 0.33 eV, 0.37 eV, 0.44 eV and 0.58 eV can be identified in the as-irradiated sample. Apart from the level at 0.18 eV, which likely belongs to the Ti on the cubic site, the other levels are unstable. These defects are potentially related to carbon interstitials (C_i) and their concentration is reduced with each 25 K increment in temperature. The 0.33 eV and 0.44 eV levels are reduced significantly after annealing at 375 K while the S1 (0.37-0.4 eV) and S2 (0.7 eV) levels are observed clearly only after the 375 K annealing. In the subsequent rounds of measurements and annealing, the concentration of S1 and S2 levels reduces (Fig. 5 b)) and are only weakly visible in the spectrum after the 650 K anneal (Fig. 5 c)). As the concentration of the defects is reduced, the free carrier concentration increases from 6.44×10^{14} cm^{-3} to 1×10^{15} cm^{-3} after the last measurement run to 700 K. This increase in the carrier concentration is taken into account while calculating the defect concentration for each run (see Table 3). The activation energy, apparent capture cross section extracted from the Arrhenius plot and the reduction in trap concentration after each run are summarized in Table 3. The $Z_{1/2}$ level at around 0.64-0.68 eV develops clearly for both sample types after annealing at 400 K. The $Z_{1/2}$ is also slightly reduced likely due to the annihilation with migrating C_i. DLTS runs to higher tem-

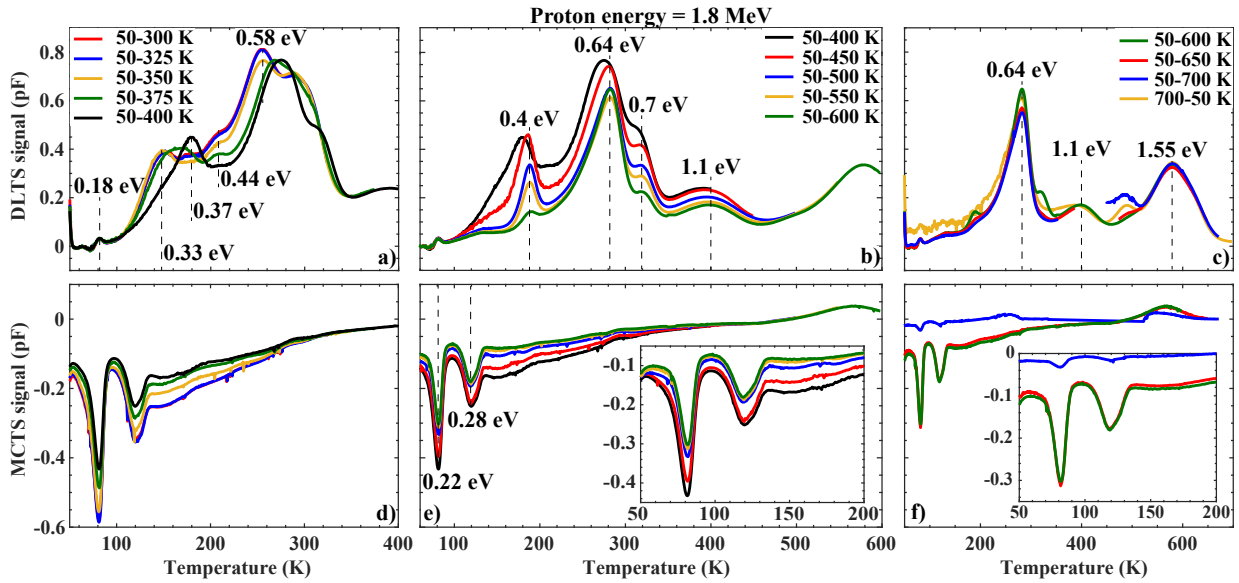

Fig. 5: DLTS (a-c) and MCTS (d-f) spectra recorded for 4H-SiC Schottky diodes irradiated with 1.8 MeV protons and a fluence of 8×10^{11} cm^{-2}.

Table 2: Summary of the defects observed using DLTS after 200 MeV proton irradiation, including energy level (eV) below the conduction band edge, capture cross section (cm^2), and the trap concentration (cm^{-3}) for each defect level and sample.

E_C-E_T (eV)	σ_{app} (cm^2) ($\times 10^{-15}$)	60-400 K ($\times 10^{13}$)	60-500 K ($\times 10^{13}$)	60-600 K ($\times 10^{13}$)	60-700 K ($\times 10^{13}$)
0.4	~1.5	-	1.25	0.78	-
0.66	~1.2	1.52	-	-	-
0.68	~15	-	1.52	2.04	1.85
0.7	~1.2	-	1.91	1.51	-
1.03 ± 0.01	~20	-	2.24	1.81	1.42
1.05 ± 0.01	~4.0	-	-	1.52	1.20

perature (>400 K) reveal the $EH_{4/5}$ (1.1 eV) and $EH_{6/7}$ (1.55 eV) peaks. The concentration of $EH_{4/5}$ reduces in each run as seen in Fig. 5 b) while the $EH_{6/7}$ level remains almost constant (Fig. 5 c)).
The MCTS spectra are shown in Fig. 5(d-f) and show two dominant peaks at 0.22 eV and 0.28 eV above the valence band edge. The 0.28 eV peak is often associated with the shallow boron level on the Si [14]. The concentration of both the minority carrier traps is steadily decreasing after each run until 600 K. Between 600-650 K, the concentrations of the defect levels remain almost constant and then reduce to a very small value in the last round of measurement up to 700 K. Additionally, the shoulder of the 0.28 eV peak also decreases after each run.

Conclusion

In this work, we have performed a study of the impact of proton irradiation on the performance of Schottky diodes using I-V measurements with forward/reverse bias and delved into the defects created by low and high energy protons using DLTS. The I-V measurements reveal that upon irradiation with 200 MeV protons, the ideality factor is improved for both the samples with Ni and Ti as the Schottky contact. Further, a reduction in the threshold voltage and an increase in the built in potential was observed. With reverse voltage measurements, an increment in the breakdown voltage after irradiation with 200 MeV protons was found. DLTS measurements on these samples reveal the presence of several defect levels in the bandgap. According to the SRIM simulations, the 200 MeV proton irradiation creates defects in the entire sample, which could be responsible for the improvement of the

Table 3: Summary of the defects observed using DLTS and MCTS after 1.8 MeV proton irradiation, including energy level (eV) below the conduction band edge (top table) or above the valence band edge (bottom table), capture cross section (cm^2), and the trap concentration (cm^{-3}) for each defect level and sample.

E_C-E_T (eV)	σ_{app} (cm^2) ($\times 10^{-15}$)	20-300 K ($\times 10^{13}$)	20-350 K ($\times 10^{13}$)	20-450 K ($\times 10^{13}$)	20-600 K ($\times 10^{13}$)	20-700 K ($\times 10^{13}$)
0.18	~21.7	4.5	4.5	4.5	4.5	4.5
0.33±0.01	~3.5	5.8	5.7	-	-	-
0.36 ± 0.01	~0.5	5.3	4.9	-	-	-
0.40 ± 0.02	~3.0	-	-	6.1	1.8	-
0.45 ± 0.01	~2.0	5.8	5.4	-	-	-
0.58	~6.1	9.3	8.8	-	-	-
0.64 ± 0.01	~4.0	-	-	8.6	7.6	8.1
0.7 ± 0.02	~1.7	-	-	4.8	2.7	-
1.05 ± 0.05	~5.0	-	-	2.4	2.0	2.1
1.55 ± 0.03	~200	-	-	-	3.4	3.9

E_V+E_T (eV)	σ_{app} (cm^2) ($\times 10^{-13}$)	20-300 K ($\times 10^{13}$)	20-350 K ($\times 10^{13}$)	20-450 K ($\times 10^{13}$)	20-600 K ($\times 10^{13}$)
0.22	~12.5	3.13	3.33	2.47	2.32
0.27 ± 0.01	~0.13	3.96	3.09	1.76	1.26

diode characteristics. DLTS measurements on the low (1.8 MeV) energy proton irradiated samples reveal that similar defect levels are generated after both the low and high energy proton irradiation. However, in spite of 6 times smaller fluence during the low energy irradiation, significantly higher defect concentrations are observed in the DLTS spectrum in comparison to the high energy protons. By slowly increasing the measurement temperature range, the impact of low-temperature annealing on the defect levels was shown. Several defects are observed in the first DLTS measurement up to room temperature which are annealed out upon exposing the sample to 400 K. The S1 and S2 levels become clear in the spectrum only after the 375 K anneal and decrease to around the DLTS detection limit after 600 K anneal. The MCTS spectrum also shows reduction in the defect concentration after each run.

References

[1] T. Kimoto and J. A. Cooper, Fundamentals of silicon carbide technology: growth, characterization, devices and applications. John Wiley & Sons (2014).
[2] F. Nava, *et al*., Materials Science Forum, Vols. 353-356, (2001), p. 757-762.
[3] Z. Luo, *et al*., IEEE transactions on nuclear science 51.6, (2004), p. 3748-3752.
[4] C. Shuang, *et al*., In 2020 IEEE 5th International Conference on Integrated Circuits and Microsystems (ICICM), (2020), p. 81-84.
[5] N. Iwamoto, *et al*., Semiconductors and Semimetals. Vol. 91. Elsevier, (2015), p. 369-407.
[6] M. E. Bathen, *et al*., npj Quantum Information 5.1 (2019): 1-9.
[7] A. Siddiqui, *et al*., Materials Science in Semiconductor Processing 135, (2021): 106085.
[8] J. Vobecky, *et al*., Solid-State Electronics 94 (2014): 32-38.
[9] S. Weiss, *et al*., Solid-State Electronics 31.12 (1988): 1733-1742.
[10] A. Castaldini, *et al*., Journal of Applied Physics 98. no. 5, (2015): 053706.
[11] E. Omotoso, *et al*., Surface and Coatings Technology, 355 (2018). p. 2-6.
[12] N.T. Son, *et al*., Physical review letters 109.18 (2012): p. 187603.
[13] R. Karsthof, *et al*., Physical Review B 102.18 (2020): p. 184111.
[14] I. Capan, *et al*., Crystals 9.7 (2019). p. 328.